Simultaneous Ultrasound Imaging Velocimetry (UIV) and Flow Visualization in Taylor-Couette flows

Validation of UIV in single-phase flows

Dash, Amitosh; Anantharaman, Arjun; Greidanus, Arnoud; Poelma, Christian

DOI
10.18726/2019_3

Publication date
2019

Document Version
Final published version

Published in
Proceedings of the 13th International Symposium on Particle Image Velocimetry (ISPIV 2019)

13th International Symposium on Particle Image Velocimetry – ISPIV 2019
Munich, Germany, July 22-24, 2019

Simultaneous Ultrasound Imaging Velocimetry (UIV) and Flow Visualization in Taylor-Couette flows: Validation of UIV in single-phase flows

Amitosh Dash[1*], Arjun Anantharaman[1], Arnoud Greidanus[2], Christian Poelma[1]

[1] Multiphase Systems, Process & Energy, Mechanical, Maritime and Materials Engineering, 2628CD Delft, The Netherlands

[2] Fluid Mechanics, Process & Energy, Mechanical, Maritime and Materials Engineering, 2628CD Delft, The Netherlands

[*] a.dash@tudelft.nl

Abstract

Ultrasound Imaging Velocimetry (UIV) is applied to a Taylor-Couette flow, for the case of pure inner cylinder rotation. By imaging a radial-azimuthal plane, two velocity components are obtained simultaneously in a two-dimensional plane. For the single-phase flow studies, Iriodin flakes (commonly used for visualizing flow structures) are used as "flow tracers" for the backscatter of ultrasound. This allows for a simultaneous mapping of the flow regime, via flow visualization, as well as extracting quantitative velocity information in the radial gap. After validating UIV against the analytically well-defined laminar Circular Couette flow as well as turbulent Taylor-Couette flow, other regimes are probed as well, in particular, the Wavy Vortex flow. Finally, the application of UIV to a particle-laden Taylor-Couette flow (particle volume fraction, $\phi \sim 0.01$) is considered, under the conditions of oscillatory pure inner cylinder rotation. The results presented here serve as a proof-of-concept for the application of UIV to the Taylor-Couette flow and will be applied to denser particle-laden flows ($\phi \sim 0.05$) in the future.

1 Flow regimes in Taylor-Couette: Pure inner cylinder rotation

The Taylor-Couette flow is a canonical flow system that has been widely studied over the last century. It is a simple system where the fluid is contained between two co-axial, independently rotating cylinders, a schematic interpretation of which is shown in Figure 1. This simple, yet well-defined flow geometry facilitates the investigation of instabilities, non-linear dynamics and spatiotemporal chaos, pattern formation and turbulence (Grossmann et al. (2016)).

Early work, such as the famous study by Taylor (1921), established the transition of Circular Couette Flow (pure azimuthal motion of fluid) to axisymmetric Taylor Vortex Flow. Since then several studies have built up and established knowledge and features of the several flow regimes that exist owing to the multiple instabilities (Coles (1965), Fenstermacher et al. (1979), Gorman and Swinney (1982), King et al. (1984), Marcus (1984)). Andereck et al. (1986) summarized the different flow regimes that can be observed in the case of a pure inner cylinder rotation as: Circular Couette Flow (CCF) $\rightarrow$ Taylor Vortex Flow (TVF) $\rightarrow$ Wavy Vortex Flow (WVF) $\rightarrow$ Modulated Wavy Vortex Flow (MWVF) $\rightarrow$ Turbulent Taylor Vortex Flow (TTVF).

Regime classification in single-phase Taylor-Couette flows is often performed by means of adding foreign elements into the working fluid, for example Kalliroscope, pearlescent pigments or rheoscopic fluids (Borrero-Echeverry et al. (2018)). These elements allow for a clear visualization of the topology of the flow structures. However, the amount of quantitative information extractable from snapshots of such flows is usually limited to characteristics of the flow features (for example, wavelengths, wave frequencies, structure

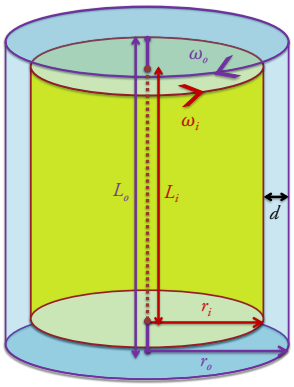

Figure 1: Schematic interpretation of the Taylor-Couette geometry

orientation etc.). Over the course of time, hot wire/film anemometry (Smith and Townsend (1982), Lewis and Swinney (1999)), Laser Doppler Anemometry (Fenstermacher et al. (1979), Burin et al. (2010)) as well as Particle Image Velocimetry (Tokgoz et al. (2012), Huisman et al. (2013)) have been deployed to study the velocity profiles in single-phase Taylor-Couette flow.

The aforementioned experimental techniques have matured and are very suitable for studying highly turbulent single-phase flows. However, applying these optical techniques to non-dilute particle-laden flows ($\phi > 0.01$) can already be complicated due to data drop-out (Deen et al. (2002), Poelma et al. (2006)). Refractive Index Matching is a potential solution and it even allows the investigation of extremely dense suspensions (Wiederseiner (2010)). However, a major limitation of this technique is the additional constraint imposed on the particle-fluid combination, disallowing the study of systems in their natural state.

Ultrasound based velocimetry is an alternative technique that can be applied to study, both, single-phase as well as particle-laden flows. This modality appears in various variants, such as Ultrasound Doppler Velocimetry (Takeda (1986)), Ultrasonic Speckle Velocimetry (Manneville et al. (2004)) and Ultrasound Imaging Velocimetry (Poelma (2017)).

Of the above three variants, Ultrasound Doppler Velocimetry was developed the earliest and provides possibilities to record a single component of velocity along a single line. Similarly, Ultrasound Speckle Velocimetry can extract a single component of velocity on a two-dimensional plane, following a calibration. For rheometric applications, for which USV was originally developed, a single velocity component is usually sufficient. Ultrasound Imaging Velocimetry (UIV), also known as "echo-PIV", applies the principles of Particle Image Velocimetry (PIV) to ultrasound images. An advantage of UIV over its other ultrasonic velocimetry counterparts is that it offers potential to measure two components of velocity simultaneously on a two-dimensional plane, and can also derive turbulence statistics (Gurung and Poelma (2016)). It should be noted that UIV does not require a calibration procedure, except for an accurate estimate for the speed of sound in the medium.

In this study, we initially revisit the classical single-phase Taylor-Couette flow, under the conditions of pure inner cylinder rotation, by combining simultaneous measurements via UIV and flow visualization. After validating the laminar velocity profile in the Circular Couette Flow regime as well as Turbulent Taylor Couette flow, UIV is combined with flow visualization to study the dominant peak frequencies occurring in the Wavy Vortex Flow regime. Finally, as a proof-of-concept, we apply UIV to a particle-laden Taylor-Couette flow (particle volume fraction, $\phi \sim 0.01$), wherein the inner cylinder undergoes a sinusoidal motion. In the future, UIV will be applied to dense particle-laden flows (particle volume fraction, $\phi \sim 0.05$), along with simultaneous flow visualization and torque measurements.

2 Experimental apparatus

Three major components were involved in the experiments: the Taylor-Couette system, the apparatus to perform UIV and the apparatus to perform flow visualization. Each of these components is described in the following subsections.

2.1 Taylor-Couette geometry

The geometry of the Taylor-Couette system used in the current experiments is summarized in Table 1. The aspect ratio of the setup is 21.67, which is considered to be high and allows for the reduction of end-effects (disturbances induced by secondary flows created by the von-Kárman gaps between the end-plates of the inner and outer cylinder). The two cylinders can be rotated independently via two Maxon DC motors. Each cylinder can rotate up to a maximum of 10 Hz with a resolution of 0.01 Hz. A torque meter (HBM T20WN, 2Nm) is used to record the torque at a sampling rate of 2 kHz. Further details of the setup can also be found in Tokgöz (2014).

Specification	Measure [units]
Inner cylinder radius (r_i)	0.11 [m]
Outer cylinder radius (r_o)	0.12 [m]
Gap width ($d = r_o - r_i$)	0.01 [m]
Radius ratio ($\eta = r_o/r_i$)	0.917 [-]
Inner cylinder length (L_i)	0.2167 [m]
Outer cylinder length (L_o)	0.2221 [m]
Aspect ratio ($\Gamma = L_i/d$)	21.67 [-]

Table 1: Specifications of the Taylor-Couette geometry for the current experiments.

2.2 Ultrasound Imaging

Ultrasound imaging is performed via a SonixTOUCH Research (Ultrasonix/BK Ultrasound) system coupled with a linear array transducer (L14-5/38). The array has 128 elements that span $\sim$3.9 cm. The imaging depth is maintained at 2 cm, allowing for a frame rate (rate at which ultrasound images are recorded) of 130 Hz. Higher frame rates, up to 400 Hz, can be obtained by reducing the imaging width/sector (lateral field-of-view) as well as reducing the line density (i.e. resolution in the lateral direction). The emitted ultrasonic pulse has a central frequency of 10 MHz and is one cycle long, while the received echo is sampled at a frequency of 40 MHz. The central frequency and the pulse cycle length determine the axial resolution of the image ($O(0.1$ mm$)$) while the sampling frequency (along with the speed of sound in the imaged medium) determines the axial spacing in the image ($O(10\mu$m$)$). This implies that the image can be downsampled/decimated in the axial direction without loss of relevant information. Raw RF signals were acquired and processed externally. In order to visualize the single-phase flow, Iriodin flakes are used as scatterers of sound, whereas the particles in the particle-laden flow act as scatterers in the two-phase flow measurements.

2.3 Flow visualization

To visualize the flow structures in an aqueous glycerol solution (56% v/v), Iriodin 100 silver pearl (Merck KGaA, Darmstadt, Germany) was added 0.1% by mass. The combination of an LaVision Imager s-CMOS camera and a Nikkon 105mm f/2.8 FX AF MICRO-NIKKOR 105 mm lens ($f_\# = 5.6$) is used at a fixed imaging rate of 32.5 Hz, with the camera focussed at the surface of the outer cylinder. Illumination is provided by means of a halogen lamp mounted above the camera. The field-of-view is a window of 10.2 $\times$ 12.08 cm^2 (axial $\times$ lateral) with the resolution in the axial direction of 21 pixels/mm. The field-of-view is located sufficiently in the centre along the axial direction in order to minimize the end effects due to the von-Karman gaps, formed between the end plates of the inner and outer cylinder (Greidanus et al. (2015)).

3 Data processing

Three types of measurements are performed on the Taylor-Couette flow: measurement of the torque required to maintain the desired rotation speed of the inner cylinder, ultrasound imaging for UIV and recording images to identify the flow regime. Results from only the latter two are presented in this paper. The procedure for processing the data is explained in brief in the following subsections.

3.1 UIV

The recorded ultrasound images were downsampled in the axial direction by a factor of four in order to reduce the inherent resolution mismatch in the imaging plane (the lateral resolution is an order of magnitude worse). This results in an image of size 228 $\times$ 128 pixels. A temporal high-pass filter is used to reduce reflections near the walls of the cylinders (Sciacchitano and Scarano (2014)). For time-averaged information, correlation-averaging multi-pass PIV is performed, with a final window size of 8 $\times$ 16 pixels with 50% overlap between the windows. The resulting spatial resolution of the velocity vectors is thus 0.7 $\times$ 4.8 mm^2. The normalized median test (Westerweel and Scarano (2005)) is used for removing outliers in space, followed by a correction to compensate for beam sweep effects (Zhou et al. (2013)). To study transient flows, a sliding moving average over 10 frames is used, resulting in effective temporal resolutions as low as 25 ms.

3.2 Flow visualization

Space-time plots are generated by stacking the scattered light intensities profiles along the centre of the image in time. Due to a skewed illumination, an intensity normalization correction is performed along the axial direction following which power spectra are then extracted from these space-time plots. The spectra are especially useful in determining the characteristic frequencies in the Wavy Taylor Vortex Flows.

4 Application of UIV to single-phase Taylor-Couette flows

Before applying UIV to particle-laden flows, it is applied to single-phase flows, which has been studied rigorously over the past decades. As a first step, the fidelity of UIV is checked on laminar Circular Couette flow as well as the Turbulent Taylor Couette flow. Hereafter, it is applied to a well defined flow regime, the Wavy Taylor Vortex regime. Here, results from UIV are also compared with those from flow visualization.

4.1 Validation: Circular Couette Flow

UIV is first applied to a low-speed laminar flow. For the Taylor-Couette system, the Couette flow velocity profile is analytically defined (Koschmieder (1993)). For pure inner cylinder rotation, the azimuthal velocity can be expressed as per Equation (1). The other velocity components (axial and radial) are expected to be zero.

$$v_\theta(r) = \left(\frac{\omega_i r_i}{1-\eta^2}\right)\left(\frac{r_i}{r} - \eta^2 \frac{r}{r_i}\right) \tag{1}$$

The results obtained by UIV on a laminar flow are shown in Figure 2. The inner cylinder had a rotation speed of approximately 7.6 cm/s leading to the inner cylinder Reynolds number ($Re_i = \frac{\omega_i r_i d}{\nu}$) of about 63. In Figure 2(a), the time-averaged velocity vectors are displayed, which are typical of a smooth, laminar, purely azimuthal flow. Two coordinate axes are shown: one based on the imaging plane (origin at one end of the ultrasound transducer), and the other based on the center of the Taylor-Couette system (i.e. cylindrical coordinates). It can be qualitatively seen that the vectors near the location $x_{cylinder} = 0$ are of better quality than those at the edges. Thus, for a quantitative analysis, vectors in a small sector near this area are considered.

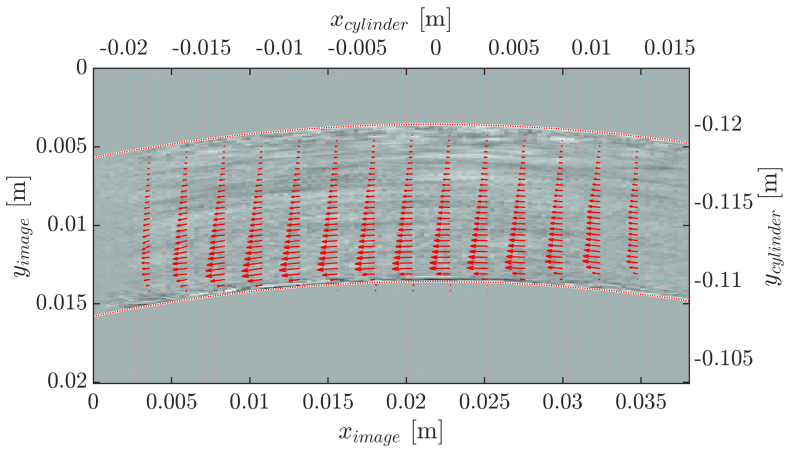

(a) Time-averaged velocity vectors. The dotted red lines indicate the cylinder walls.

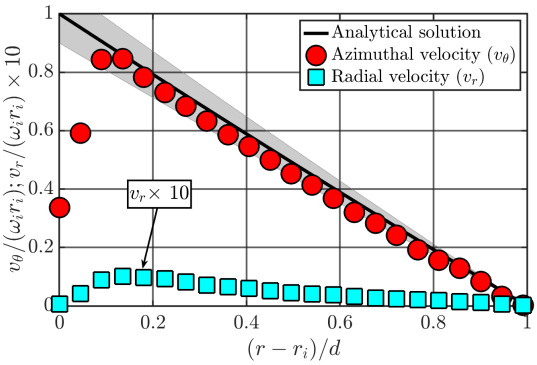

(b) Mean azimuthal and radial velocities (normalized by the inner cylinder velocity). Note that absolute values have been plotted.

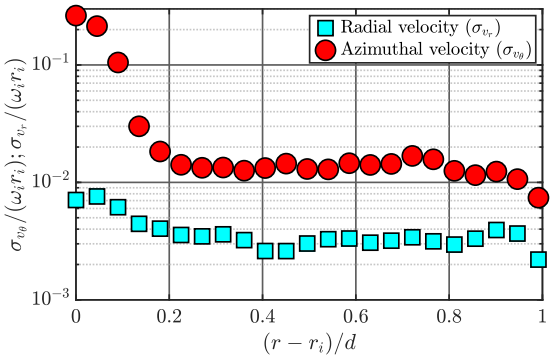

(c) Standard deviation of the azimuthal and radial velocities (normalized by the inner cylinder velocity).

Figure 2: Velocities obtained in a laminar Circular Couette Flow at $Re_i \sim 63$. Solid black line in (a) represents the analytical solution whereas the patch is $\pm 10\%$ deviation from the analytical solution. Note that the statistics corresponding to the radial velocity components are multiplied by a factor of ten for better visualization.

The mean azimuthal and radial velocities for this flow are shown in Figure 2(b). The measured azimuthal velocities are in good agreement with the expected analytical profile until $(r - r_i)/d > 0.15$. Closer to the inner cylinder, velocities are miscalculated due to curvature effects, and also relatively higher particle displacements. The PIV grid is rectangular, and near the cylinder walls, part of the interrogation window lies outside the system. This leads to an underestimation of the particle displacements, and thus the velocities. A possible solution is performing cross-correlation on a conformal grid (Nguyen et al. (2010), Park et al. (2015)). Maximum mean radial velocities of up to 1% of the inner cylinder velocity are observed even though these are expected to be zero. This is an indication of the maximum accuracy of the technique with respect to the mean radial velocities.

The instantaneous azimuthal and radial velocities were also computed for this flow, which allowed the calculation of their respective standard deviations, plotted in Figure 2(c). For a pure laminar flow, these quantities should be zero. However, this is not observed and the deviations serve as an indicator for the maximum accuracy of the technique for temporally varying flows. Variations up to 2% and 0.5% of the inner cylinder velocity are observed for the azimuthal and radial velocity components in the bulk of the flow. A possible reason for this might be the disparity in the spatial resolution in the two directions. This also implies that the fluctuations of the radial velocity component would be a better indicator for the level of turbulence in the flow.

4.2 Validation: Turbulent Taylor Couette Flow

Following the study of the laminar Circular Couette Flow, other flow regimes obtainable at higher Re_i are considered. Higher Reynolds numbers are obtained here by increasing the speed of the inner cylinder rotation, as well as reducing the viscosity of the working fluid. It is known that UIV performed on images acquired by traditional beamforming can typically resolve velocities up to 0.8 m/s (Poelma (2017)). Thus, one might anticipate that this would impose an upper bound on the maximum resolvable azimuthal velocities. However, it is also known that in non-laminar flows, a relative flattened profile for the azimuthal velocity is obtained in the bulk, and is typically ∼50% of the inner cylinder velocity (Wereley and Lueptow (1994)). This fact allows for studying flows driven by even higher inner cylinder velocities, at least in the bulk.

For validation at higher velocity ranges, as well as a higher Reynolds number, a measurement was performed in a flow where the inner cylinder was rotated at a speed of 1.46 m/s resulting in $Re_i = 1.46 \times 10^4$. The azimuthal velocities are compared with those measured by Ravelet et al. (2010) in the same facility using Stereoscopic PIV at a flow with a comparable Reynolds number ($Re_i = 1.4 \times 10^4$).

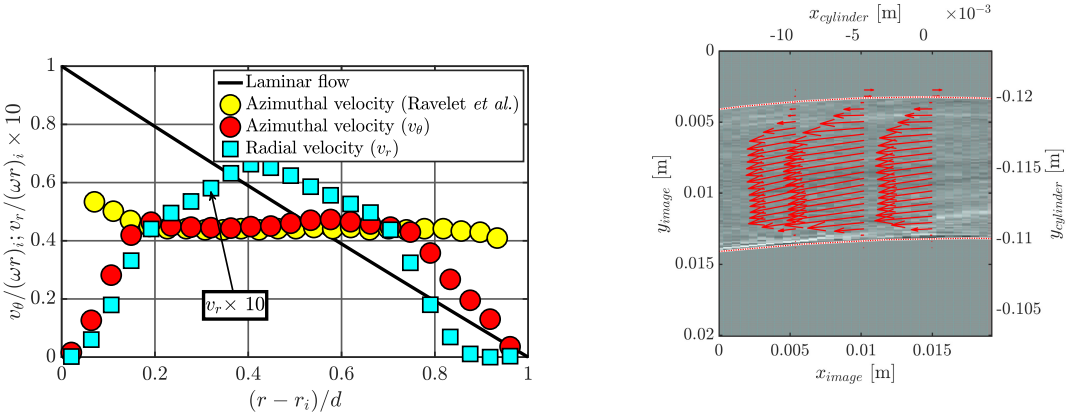

(a) Mean azimuthal and radial velocities (normalized by the inner cylinder velocity). Note that absolute values have been plotted.

(b) Time-averaged velocity vectors. The dotted red lines indicate the cylinder walls.

Figure 3: Velocities obtained in a turbulent Taylor Couette Flow at $Re_i \sim 1.4 \times 10^4$. Current results are compared with the PIV measurements of Ravelet et al. (2010). Note that the statistics corresponding to the radial velocity components are multiplied by a factor of ten for better visualization.

It can be seen in Figure 3(a) that there is a good agreement between the two measurements of azimuthal velocities in the central region ($0.2 \leq (r - r_i)/d \leq 0.75$). However, there is a significant deviation in the regions closer to the cylinder walls. There are a few possible reasons for this. The PIV results have been averaged over an axial distance, as compared to the UIV results which correspond to a local axial location. This also means that the current UIV measurements are sensitive to the axial placement of the transducer with respect to a single Taylor roll as well as the Reynolds number of the flow. The Taylor rolls may change their location with changing Reynolds numbers and thus, it would be cumbersome to place the transducer consistently at the center, inflow or outflow of a Taylor roll. For example, the time-averaged velocity vectors in Figure 3(b) indicate that the transducer is located relatively closer to an inlet of the Taylor roll (due to the inward motion of the fluid). The measured radial velocity component profile is qualitatively typical of profiles measured in other studies, albeit with differing flow geometries (Bilson and Bremhorst (2007)).

4.3 Comparison with Flow Visualization: Wavy Taylor Vortex Flow

Next, we compare results from UIV as well as flow visualization, whose measurements were performed simultaneously. We focus on the Wavy Taylor Vortex Flow regime which is characterized by waves travel-

ling in the azimuthal direction. Power spectra of the light intensity (recorded at a fixed axial location via flow visualization) and radial velocity fluctuations (measured via UIV) are computed. In the wavy vortex flow regime, a distinct peak (f_{peak}) is present in the power spectra, which corresponds to the periodicity of the travelling waves (Fenstermacher et al. (1979)). These peak frequencies (normalized by the rotational frequency of the inner cylinder, f_i) measured by the two techniques are then compared for varying inner cylinder Reynolds numbers.

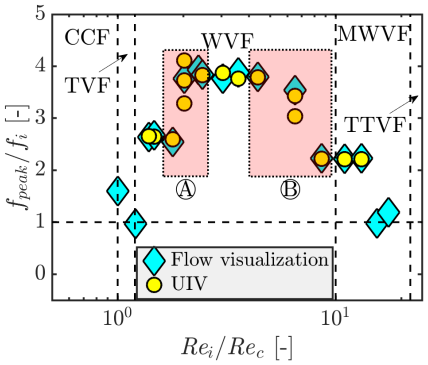

(a) Comparison of the peak frequencies measured by the two techniques.

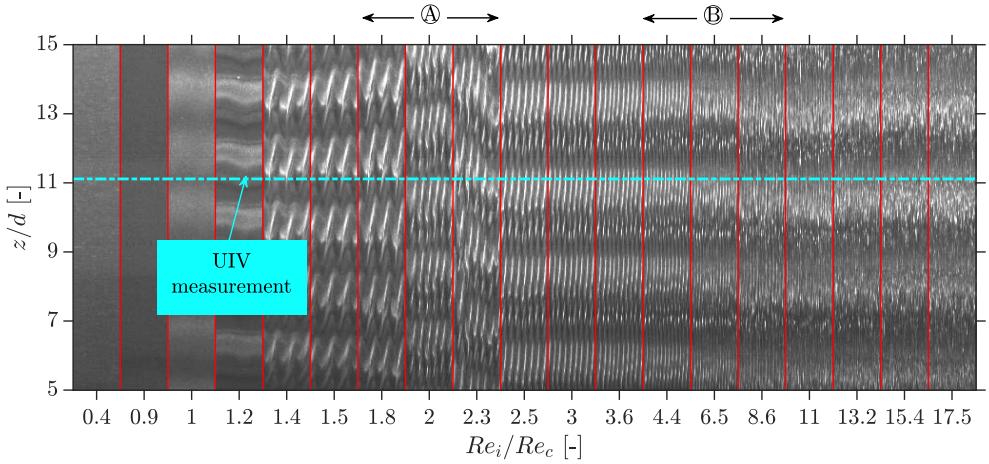

(b) Space-time plots of the scattered light intensity for various Reynolds numbers.

Figure 4: Transition within the Wavy Vortex Flow regime as captured by flow visualization and UIV. Regime demarcation in (a) is based on the measurements of Fenstermacher et al. (1979).

This comparison can be seen in Figure 4(a). Shown also are demarcation of flow regimes observed by Fenstermacher et al. (1979) in their measurements, albeit for a system with $\eta = 0.877$. The critical Reynolds number Re_c is the Reynolds number at which the first instability occurs (CCF $\rightarrow$ TVF), which in the current case is ≈ 134, as seen by flow visualization. This is 8% lower than the analytically predicted value by Esser and Grossmann (1996). Both measurement techniques reveal a similar behaviour of the peak frequencies. A sudden shift in the plateau for f_{peak}/f_i can be seen around $Re_i/Re_c \sim 2$ and ~ 6.5 (denoted by Ⓐ and Ⓑ respectively in Figure 4). The first transition Ⓐ represents a shift in the spatial state of the system, in the axial direction, i.e. there is an increase in the number of Taylor rolls in the axial direction. The second transition Ⓑ possibly represents the scenario in which there is a change in the number of waves along the azimuthal direction. Both measurement techniques provide similar results, which is in accordance with Gorman et al. (1980) who showed that different methods of probing resulted in similar power spectra. Currently, we have not detected a secondary peak in out power spectra that would be expected in the MWVF regime. This will be looked into in more detail in future studies.

5 Application of UIV to particle-laden Taylor-Couette flow

Finally, we apply UIV to a particle-laden Taylor-Couette flow in which Polystyrene spheres (diameter $\sim$ 530 $\pm$ 75 μm, specific gravity $\sim$ 1.04) were added to an aqueous Glycerol solution (specific gravity $\sim$ 1.23) to form a suspension with a volume fraction of 1%. UIV has previously been successfully applied to such particle-laden flows (Gurung and Poelma (2016), Hogendoorn and Poelma (2018)). In the suspension studied here, a significant effect of buoyancy is expected on the particles, leading to an expected rise velocity of approximately 0.43 mm/s. This rise velocity, however, is not expected to cause a significant out-of-plane motion of particles between two consecutive frames. The focus of the current measurements is to check the fidelity of UIV by measuring the azimuthal velocity.

The inner cylinder is oscillated, while the outer cylinder is kept fixed. This leads to an inner cylinder velocity profile $U_i(t) = U_{base} + U_{ampl} \cdot \sin(\frac{2\pi t}{T})$. The inner cylinder velocity (U_i) is defined by a base velocity (U_{base}), an amplitude (U_{ampl}) and a time period (T). For the current case, we consider the case with $T = 3s$ and $U_{base} = U_{ampl} = 0.17m/s$. The instantaneous Reynolds numbers thus vary between 15 $\pm$ 15, which implies under single-phase flow conditions the flow would always remain laminar for which an analytical solution for the azimuthal velocity profile can be calculated (Verschoof et al. (2018)). This flow is thus more challenging to measure than a pure Circular Couette Flow, and at the same time has a well-defined theoretical velocity profile. This is in contrast with flows with Taylor vortices, where a clear quantitative reference for the velocities is not easily available.

For the current studies, the Womersley number (ratio between the unsteady inertial forces and viscous forces), $Wo \sim O(1)$. Under these conditions, it is expected that the working fluid perfectly follows the modulations created by the inner cylinder (Verschoof et al. (2018)). Since the particle Stokes number $\ll 0.1$ (characteristic time scale of fluid $\sim d/U_{base}$, since the flow is laminar), it can also be expected that the particles more or less respond to the accelerations/decelerations of the fluid. It should be noted that UIV returns the velocities of the dispersed phase and not the fluid carrying the particles.

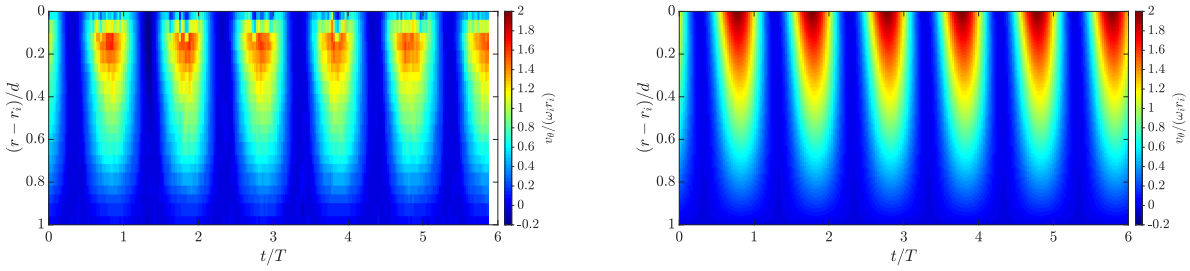

(a) Azimuthal velocities measured by UIV.

(b) Azimuthal velocities calculated analytically.

Figure 5: Application of UIV to a particle-laden Taylor-Couette flow. The inner cylinder is modulated with a time period of $T = 3s$.

Space-time plots of the azimuthal velocity obtained experimentally and analytically are plotted in Figure 5(a) and Figure 5(b) respectively. A good qualitative agreement is visible between the plots, especially for $(r-r_i)/d > 0.15$. The relatively low Womersley number implies that the Stokes boundary layer thickness is much larger than the gap width d. This is also visible in the space-time plots as the peak velocities of the cylinder are propagated almost immediately over the gap.

6 Conclusion: UIV is a potential tool for particle-laden Taylor-Couette flows

In this paper, we applied UIV to single-phase Taylor-Couette flows driven by pure inner cylinder rotation and validated the mean velocity fields under both, the laminar and turbulent regime. It is also indicated that the radial velocity fluctuations are more appropriate for studying the turbulent characteristics of the flow.

A good correlation was obsered in the qualitative behaviour of the peak frequencies calculated from the power spectra of the radial velocity fluctuations (UIV) and the scattered light intensity (flow visualization). Finally, as a proof-of-concept, UIV was applied to a particle-laden flow (volume fraction 0.01) with the inner cylinder modulated sinusoidally. The velocity profiles obtained were also in-line with those expected analytically. In the future, UIV shall be applied with simultaneous flow visualization and torque measurements to particle-laden flows with higher volume fractions, to extract information about the flow regime and velocity profiles simultaneously similar to the recent studies by Majji et al. (2018) and Ramesh et al. (2019).

Acknowledgements

AD and CP have received funding from the ERC Consolidator Grant 725183 'OpaqueFlows'. The authors thank Edwin Overmars, Jan Graafland and Jasper Ruijgrok for their technical assistance in setting up the experiments. Furthermore, AD would like to thank Willian Hogendoorn for many discussions on UIV.

References

Andereck CD, Liu S, and Swinney HL (1986) Flow regimes in a circular Couette system with independently rotating cylinders. *Journal of Fluid Mechanics* 164:155–183

Bilson M and Bremhorst K (2007) Direct numerical simulation of turbulent Taylor–Couette flow. *Journal of Fluid Mechanics* 579:227–270

Borrero-Echeverry D, Crowley CJ, and Riddick TP (2018) Rheoscopic fluids in a post-Kalliroscope world. *Physics of Fluids* 30:087103

Burin M, Schartman E, and Ji H (2010) Local measurements of turbulent angular momentum transport in circular Couette flow. *Experiments in Fluids* 48:763–769

Coles D (1965) Transition in circular Couette flow. *Journal of Fluid Mechanics* 21:385–425

Deen NG, Westerweel J, and Delnoij E (2002) Two-phase PIV in Bubbly Flows: Status and Trends. *Chemical Engineering & Technology* 25:97–101

Esser A and Grossmann S (1996) Analytic expression for Taylor–Couette stability boundary. *Physics of Fluids* 8:1814–1819

Fenstermacher P, Swinney HL, and Gollub J (1979) Dynamical instabilities and the transition to chaotic Taylor vortex flow. *Journal of Fluid Mechanics* 94:103–128

Gorman M, Reith LA, and Swinney HL (1980) Modulation patterns, multiple frequencies, and other phenomena in circular Couette flow. *Annals of the New York Academy of Sciences* 357:10–21

Gorman M and Swinney HL (1982) Spatial and temporal characteristics of modulated waves in the circular Couette system. *Journal of Fluid Mechanics* 117:123–142

Greidanus A, Delfos R, Tokgoz S, and Westerweel J (2015) Turbulent Taylor–Couette flow over riblets: drag reduction and the effect of bulk fluid rotation. *Experiments in Fluids* 56:107

Grossmann S, Lohse D, and Sun C (2016) High–Reynolds number Taylor-Couette turbulence. *Annual Review of Fluid Mechanics* 48:53–80

Gurung A and Poelma C (2016) Measurement of turbulence statistics in single-phase and two-phase flows using ultrasound imaging velocimetry. *Experiments in Fluids* 57:171

Hogendoorn W and Poelma C (2018) Particle-Laden Pipe Flows at High Volume Fractions Show Transition Without Puffs. *Physical Review Letters* 121:194501

Huisman SG, Scharnowski S, Cierpka C, Kähler CJ, Lohse D, and Sun C (2013) Logarithmic boundary layers in strong taylor-couette turbulence. *Physical Review Letters* 110:264501

King GP, Li Y, Lee W, Swinney HL, and Marcus PS (1984) Wave speeds in wavy Taylor-vortex flow. *Journal of Fluid Mechanics* 141:365–390

Koschmieder EL (1993) *Bénard cells and Taylor vortices*. Cambridge University Press

Lewis GS and Swinney HL (1999) Velocity structure functions, scaling, and transitions in high-Reynolds-number Couette-Taylor flow. *Physical Review E* 59:5457

Majji MV, Banerjee S, and Morris JF (2018) Inertial flow transitions of a suspension in Taylor–Couette geometry. *Journal of Fluid Mechanics* 835:936–969

Manneville S, Bécu L, and Colin A (2004) High-frequency ultrasonic speckle velocimetry in sheared complex fluids. *The European Physical Journal-Applied Physics* 28:361–373

Marcus PS (1984) Simulation of Taylor-Couette flow. part 2. Numerical results for wavy-vortex flow with one travelling wave. *Journal of Fluid Mechanics* 146:65–113

Nguyen CV, Nguyen TD, Wells JC, and Nakayama A (2010) Interfacial PIV to resolve flows in the vicinity of curved surfaces. *Experiments in Fluids* 48:577–587

Park J, Im S, Sung HJ, and Park JS (2015) PIV measurements of flow around an arbitrarily moving free surface. *Experiments in Fluids* 56:56

Poelma C (2017) Ultrasound imaging velocimetry: a review. *Experiments in Fluids* 58:3

Poelma C, Westerweel J, and Ooms G (2006) Turbulence statistics from optical whole-field measurements in particle-laden turbulence. *Experiments in Fluids* 40:347–363

Ramesh P, Bharadwaj S, and Alam M (2019) Suspension Taylor–Couette flow: co-existence of stationary and travelling waves, and the characteristics of Taylor vortices and spirals. *Journal of Fluid Mechanics* 870:901–940

Ravelet F, Delfos R, and Westerweel J (2010) Influence of global rotation and reynolds number on the large-scale features of a turbulent Taylor–Couette flow. *Physics of Fluids* 22:055103

Sciacchitano A and Scarano F (2014) Elimination of PIV light reflections via a temporal high pass filter. *Measurement Science and Technology* 25:084009

Smith G and Townsend A (1982) Turbulent Couette flow between concentric cylinders at large Taylor numbers. *Journal of Fluid Mechanics* 123:187–217

Takeda Y (1986) Velocity profile measurement by ultrasound Doppler shift method. *International journal of heat and fluid flow* 7:313–318

Taylor GI (1921) Experiments with rotating fluids. *Proceedings of the Royal Society of London Series A, Containing Papers of a Mathematical and Physical Character* 100:114–121

Tokgöz S (2014) *Coherent structures in Taylor-Couette flow: Experimental investigation*. Ph.D. thesis

Tokgoz S, Elsinga GE, Delfos R, and Westerweel J (2012) Spatial resolution and dissipation rate estimation in Taylor–Couette flow for tomographic PIV. *Experiments in Fluids* 53:561–583

Verschoof RA, te Nijenhuis AK, Huisman SG, Sun C, and Lohse D (2018) Periodically driven Taylor–Couette turbulence. *Journal of Fluid Mechanics* 846:834–845

Wereley S and Lueptow R (1994) Azimuthal velocity in supercritical circular Couette flow. *Experiments in Fluids* 18:1–9

Westerweel J and Scarano F (2005) Universal outlier detection for PIV data. *Experiments in Fluids* 39:1096–1100

Wiederseiner S (2010) *Rheophysics of concentrated particle suspensions in a Couette cell using a refractive index matching technique*. Ph.D. thesis

Zhou B, Fraser KH, Poelma C, Mari JM, Eckersley RJ, Weinberg PD, and Tang MX (2013) Ultrasound imaging velocimetry: Effect of beam sweeping on velocity estimation. *Ultrasound in Medicine & Biology* 39:1672–1681